Light Emission from Nanocrystalline Si Inverse Opals and Controlled Passivation by Atomic Layer Deposited Al_2O_3

Francisco Gallego-Gómez, Marta Ibisate, Dolores Golmayo, F. Javier Palomares, Miriam Herrera, Jesús Hernández, Sergio I. Molina, Álvaro Blanco, and Cefe López*

The discovery of photoluminescence (PL) in porous silicon[1] has triggered enormous interest in light-emitting silicon nanostructures to realize CMOS-compatible photonics (in particular, silicon lasers),[2–4] sensing[5] and biology/medicine applications.[6] Light emission from silicon nanocrystals (Si-NCs) is generally attributed to both quantum confinement of excitons and localized defect states.[7,8] Surface species at the NC interface can greatly affect the PL properties.[5,9] Nonradiative recombination at e.g. silicon dangling bonds causes emission quenching, so PL is typically unstable, especially in air and under light illumination.[10–13] In the last two decades, a wide variety of techniques for nanocrystalline Si fabrication and posterior surface stabilization have been investigated. Passivation by high-pressure water vapor annealing, thermal oxidation, coating deposition, wet chemistry, etc., has been studied (see e.g. Ref. 13 and references therein). However, a main difficulty for passivation is encountered as the nanocrystals are hardly reachable in most structures. This is the case of porous silicon films or Si-NC ensembles typically embedded in host matrices, like silica, acting as supporting media[2,8,14,15] Here we present a permeable, self-supported Si-NC structure, which can be efficiently passivated by thin alumina layers to obtain efficient and stable PL. The structure consists of an artificial inverse opal formed by microporous walls of photoluminescent Si-NCs obtained by low-temperature magnesiothermic reduction and posterior selective etching.[16] The morphology and order of the starting silica structure are retained without further processing[16–19] The three-dimensionally (3D) patterned volume of the opal and the highly porous nature of the Si-NC assembly maximize the accessibility of the nanocrystals, allowing optimized manipulation of the silicon surface. As a result, the opal PL, which otherwise exhibited extreme photodegradation, was preserved by accurate infiltration of alumina via atomic layer deposition (ALD).

The fabrication steps are summarized in **Figure 1**. Silica inverse opals, obtained from polystyrene (PS) opals, were converted into a Si/MgO replica by magnesiothermic reduction (Figure 1a). The resulting inverse opal walls consisted of bi-continuous, interpenetrating silicon and magnesia phases with 35:65 volume ratio.[16] Magnesia was completely dissolved by HCl etching, while silicon was retained as a highly porous, interconnected structure preserving the original morphology (Figure 1b). Rigorously, the opal was not only formed by silicon but also by remnant silica (unreacted during magnesioreduction or formed during exposure of silicon to the water-rich HCl solution). Silica content at this stage was estimated from energy-dispersive X-ray (EDX) spectroscopy to be ~9 vol.% of the walls. The structure was further retained by etching the silica with HF (Figure 1c), obtaining a *bare* inverse opal exclusively formed by self-supported nanocrystalline silicon. Finally, the opal was infiltrated with alumina by ALD (Figure 1d). Among oxide coatings, widely used for silicon passivation, alumina ALD has been already proved to be effective on Si-NCs[3,20] and it allowed us deposition with sub-nanometer precision. The high porosity of the Si-NC opal and the absence of supporting matrix were expected to facilitate the homogenous covering of the NCs surface throughout the opal structure.

The fabrication process was monitored by scanning electron microscopy (SEM, Figure 1), optical, x-ray photoelectron (XPS) and EDX spectroscopies. The persistence of the opal photonic stop-band in the reflection spectra was confirmed at every stage (not shown). Starting from 940 nm PS spheres, the first-order stop-bands appeared at wavelengths higher than 1700 nm. From the stop-band position after opal inversion, a wall thickness of ~45 nm was estimated, which agrees well with the SEM images. EDX confirmed the removal of Mg and silica in opals (b) and (c), respectively. In the latter opal, the formation of native silica by oxidation of silicon in air was observed (~6 vol.%, measured by EDX 2 hours after HF etching). High resolution transmission electron microscopy (HRTEM) images show the ensemble of adjacent Si-NCs in the inverse opal (d), in which different dimensions and orientations can be appreciated (**Figure 2**a). Among them, the existence of nanocrystals with size <4 nm (highlighted with circles) was directly confirmed (Figure 2b), which is a decisive aspect for the occurrence of visible PL. Previous studies on silicon structures obtained by magnesiothermic reduction reported an average size of the Si-NCs of ~13 nm,[16–18] based on Scherrer

Dr. F. Gallego-Gómez, Dr. M. Ibisate, Dr. D. Golmayo,
Dr. F. J. Palomares, Dr. Á. Blanco, Prof. C. López
Instituto de Ciencia de Materiales de Madrid and Unidad Asociada CSIC-U Vigo
Consejo Superior de Investigaciones Científicas
28049 Madrid, Spain
E-mail: ablanco@icmm.csic.es, website: luxrerum.org
Dr. M. Herrera, J. Hernández, Prof. S. I. Molina
Departamento de Ciencia de los Materiales e Ingeniería Metalúrgica y Química Inorgánica
Facultad de Ciencias
Universidad de Cádiz
11510 Puerto Real, Cádiz, Spain

DOI: 10.1002/adma.201101797

ADVANCED MATERIALS
www.advmat.de

www.MaterialsViews.com

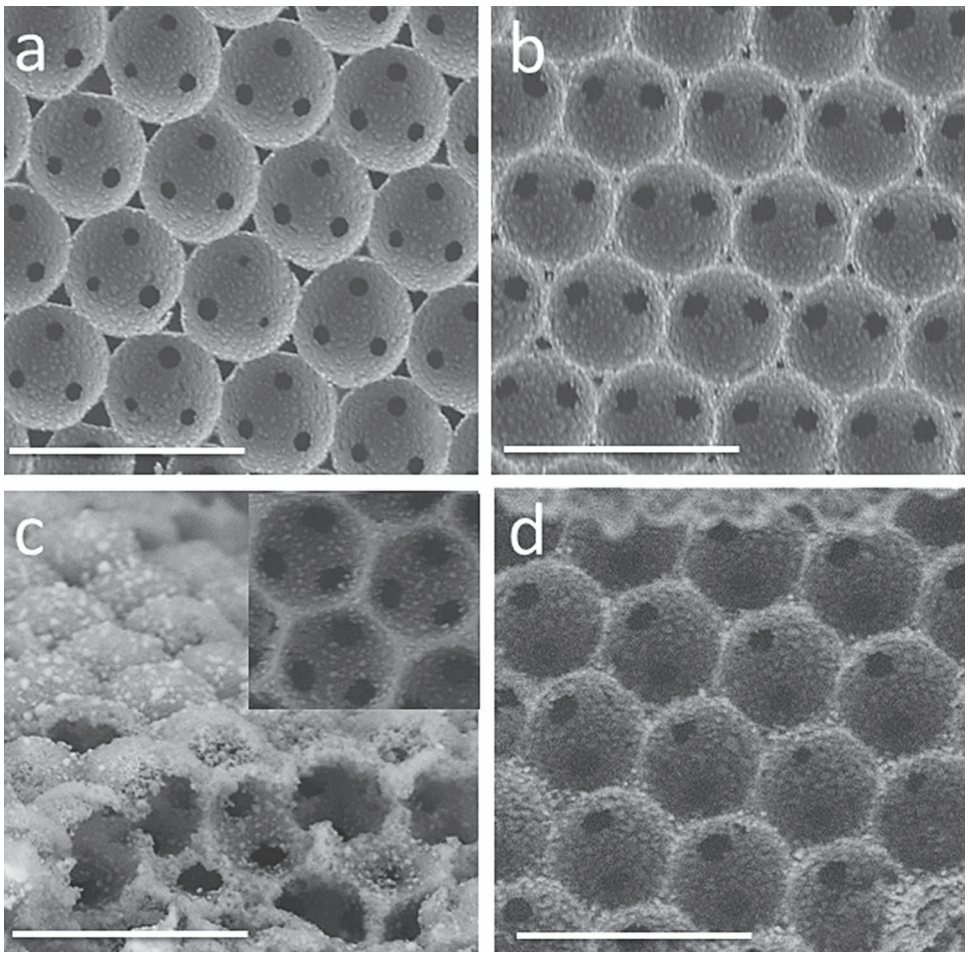

Figure 1. Fabrication process: Inverse silica opals were converted into Si/MgO replicas by magnesiothermic reduction (a). Magnesia and remnant silica were removed by selective etching with HCl (b) and HF (c), respectively. Finally, alumina was infiltrated by ALD for silicon passivation (d; image after 10 ALD cycles). SEM images of (111) opal planes taken at every stage demonstrate the preservation of the structure. Tilted image of opal (c) show the silicon foam-like walls forming the self-supported opal microstructure. Scale bar is 2 µm.

analysis from X-ray diffraction that probably underestimated the contribution of small crystallites. From TEM observations, Hatton et al. reported a Si-NC size of 5–10 nm.[19] Cai et al.[21] directly confirmed the simultaneous formation of Si and MgO nanocrystals of ~5 nm during the exposure of a silica structure to magnesium gas.

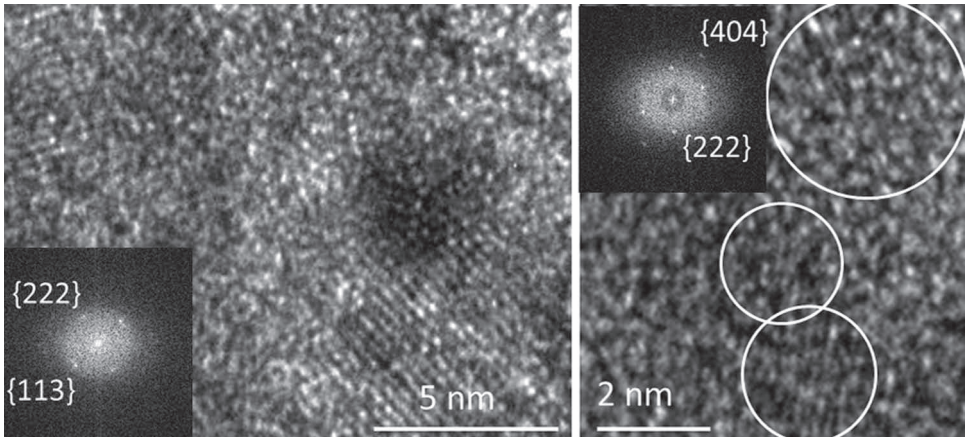

Figure 2. HRTEM images of the Si-NC ensemble in opal (c). Fast Fourier transforms (insets) emphasize the NC periodicities. Silicon atomic planes {113}, {222} and {404} are identified (corresponding to 6.1, 6.4 and 10.4 nm^{-1} inverse distances, respectively).

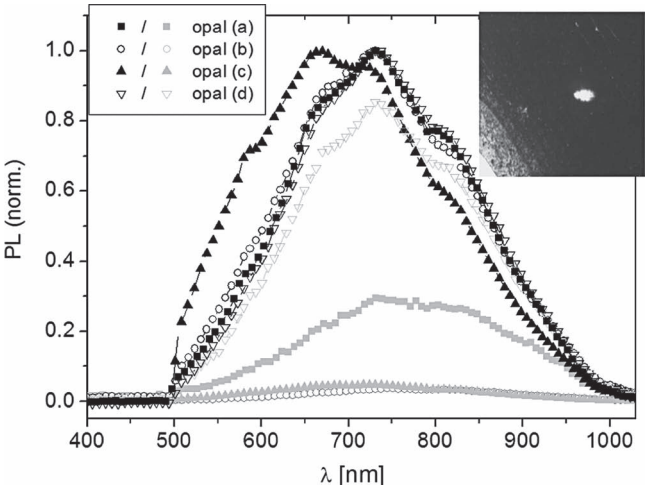

Figure 3. PL emission from opals (a)–(d), as described in Figure 1. Opal (d) was infiltrated with 10 ALD cycles. Maximum and steady-state (after irradiating for 800 ms) PL intensities are shown (solid and open symbols, respectively). PL was induced by a 488 nm laser, ~2 W/cm^2 (spectra were normalized for comparison). Inset: optical image (1.5 mm × 1.5 mm) of a photoluminescent spot (appearing as a bright spot in the image–yellow-orange in reality). Opal monolayers (from 1 to several) are observable at the lower left corner of the image.

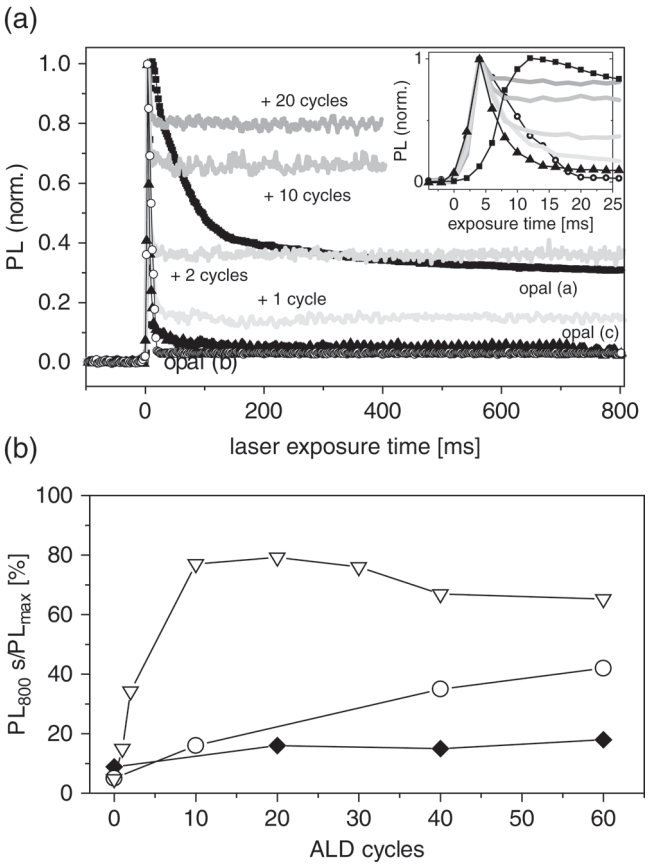

Figure 4. (a) Time evolution of PL intensity of inverse opals (a–d) upon uninterrupted photoexcitation (Ar^+ laser was switched on at t = 0). Opal (d) was infiltrated by a different number of alumina-ALD cycles. Inset: zoomed-in view of the early stages. (b) Stabilization of the PL intensity (quantified by the ratio of PL at t = 800 ms to its maximum value) by alumina infiltration. Opal (d) (open triangles) and a Si-NC non-structured film (solid diamonds) were passivated by a varying number of ALD cycles. For comparison, alumina was also infiltrated in opal (b), i.e., without HF etching (open circles).

The silicon-based inverse opals at every fabrication stage, exposed to ambient air at room temperature and without further processing, emitted in the visible-NIR range (**Figure 3**) under 488 nm photoexcitation (with intensity of ~2 W cm^{-2}, which is fairly low in this kind of systems since irradiances in the range of kW cm^{-2} have been employed in many studies–see e.g. Refs. 2, 11, 12, 22). PL emission, similarly intense in all opals, was even detectable with the naked eye (inset in Figure 3). The broad emission spectrum, typical for ensembles of silicon NCs having a size distribution (see e.g. Refs. 1, 14–16), can be attributed to excitonic emission of NCs of diameter ~2–5 nm,[8,9,23] although radiative recombination at oxide-related surface defects might also be at play.[5,7] Note that the opal photonic stop-band did not overlap with the emission spectrum, so that PL was not influenced by any photonic effect of the structure. Thus, the opal is here designed just as suitable scaffold for nanostructuring self-supported Si-NCs. By comparing the PL spectra at the different fabrication steps (Figure 3), the emission, centered at ~750 nm in the Si/MgO structure (opal (a)), progressively shifted to shorter wavelengths (up to ~680 nm) upon removing the magnesia and the remnant silica (opals (b) and (c)). By contrast, the emission shifted back upon infiltration with alumina (opal (d)). The notable shape difference of PL between (b) and (c), although having comparable silica contents, evidences the dissimilar nature of silica in both opals.

As a critical drawback, PL in opals (a)–(c) exhibited pronounced photodegradation in the ms range under continuous photoexcitation, from 30% of the maximum value in the Si/MgO opal to 96% after magnesia etching. By contrast, Al_2O_3 deposition in opal (d) drastically prevented the PL degradation, as intended, and the emission signal stabilized after a small decrease. The different covering of the Si-NCs also affected the dynamics (**Figure 4**a). PL in the opal (a) showed a relatively slow buildup (half-time, i.e., time needed to reach half the maximum, was ~8 ms) and degraded along the next 1000 ms, approximately. After removing the magnesia, the dynamics (both buildup and fade out) were much faster and the PL degradation even increased. Dynamics further accelerated after etching of the remnant silica. It must be pointed out that no significant change was observed in the PL behavior in opal (c) within 1 hour and 5 months after HF etching. This suggests that the growth of native silica in air rapidly stabilized, in accordance with the high porosity of the system. The dynamic properties demonstrate, on the one hand, that the abundant presence of MgO contributed to partial stabilization of the PL emission, probably by physical hindering of the NC-air contact. On the other hand, PL stabilization was much more effective with low amounts of alumina (less than 11 vol.% of the wall after 10 ALD cycles, as estimated by EDX). The presence of remnant silica (opal (b)) or native silica (opal (c)) did not prevent almost complete PL photodegradation.

Alumina deposition on the Si-NCs was accurately controlled by selecting the numbers of ALD cycles. We found that the PL stabilization strongly depended on the degree of infiltration. This feature was investigated on different pieces of a Si-NC inverse opal by varying the number of ALD cycles between 0 (bare opal) and 60 (Figure 4). The PL temporal evolution (Figure 4a) exhibited similarly fast buildups (half-times of ~2 ms) followed by a rapid decrease after the maximum, inevitable in all cases. The emission intensity was stable after a few tens of ms. The PL remainder (percentage of the maximum value after 800 ms) clearly improved with increasing alumina deposition, from 4% in the bare opal up to ~80% after only 10 ALD cycles (Figure 4b). PL photostability did not further improve above 10 ALD cycles, which suggests that the alumina effect did not consist only in NC encapsulation (which would be proportional to the amount of deposited alumina). In this regard, the passivation effect was observable even after one single ALD cycle, and the steady-state PL intensity improved in one order of magnitude after 2 ALD cycles.

The chemical composition of the outermost surface layers of the samples was investigated by XPS, with emphasis on the influence of the alumina deposition on the surface species (**Figure 5**). Prior to ALD, both oxide (native SiO_2) and bulk (Si^0) silicon 2*p* peaks were well separated in opal (c), similarly to what is observed in a silicon wafer (with native oxide). The 2*p* spin-orbit splitting, $p_{1/2}$ and $p_{3/2}$, was clearly resolved for the crystalline bulk silicon but not for the amorphous oxide layer. The Si/Si-oxide interface basically consisted of Si^{4+} state (at ~104 eV), as commonly observed in oxidation of silicon surfaces.[24] After alumina deposition (opal (d)), among the increase of SiO_2 emission, the formation of large amount of Si intermediate oxidation states (suboxides) at the Si-NCs surface was evident. The formation of Si^{3+} (at ~102.3 eV) shifted the SiO_2 emission to lower binding energy due to its balance with Si^{4+}. The fitting of the spectrum after a Shirley background subtraction (not shown) revealed also large amounts of Si^{1+} and Si^{2+} (at 100.7 and 101.6 eV, respectively). On the contrary, the deposition of alumina on the silicon wafer did not lead to shift of the SiO_2 emission or to appearance of suboxides. Such behavior might be attributed to the variety of dangling bonds (or facets) in the Si-NCs surface, unlike the single orientation in the silicon wafer, leading to highly disordered Si/Si-oxide interface in opal (d). The latter fact agrees with the broadening of the bulk Si emission in the opal (and not in the wafer). By contrast, the line shape analysis of the Al 2*p* core level showed only one sharp and strong peak located at the characteristic binding energy of a completely oxidized Al_2O_3, without any sign of aluminum suboxides or even metallic Al. This fact confirmed the good chemical stability of the deposited alumina layer. Again, the broader peak in the opal case indicates higher disorder in the alumina grown on the Si-NCs. The results demonstrate chemical changes at the Si-NCs interface, with formation of abundant suboxides, that might play an essential role in the efficient passivation of the opal by ALD alumina.

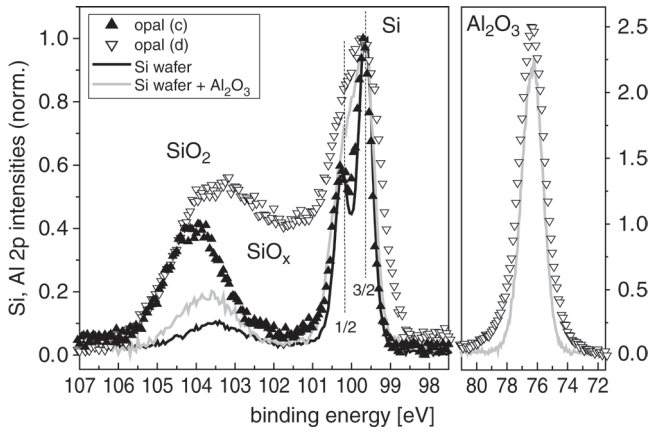

Figure 5. Si and Al 2*p* photoelectron spectra (XPS) of the Si-NC inverse opal and a silicon wafer (both having native silica) before and after alumina deposition (30 ALD cycles).

Besides, the high penetrability of the Si-NC opal was intended to enhance the accessibility to the nanocrystals, enabling surface passivation throughout the whole sample. Thus, among the high porosity of the silicon structure obtained by magnesioreduction, the 3D-nanostructuring of the thin (<50 nm) inverse opal walls would decisively improve the passivation. As a direct experimental verification of this thesis, we evaluated the PL stabilization by alumina in an equivalent Si-NCs ensemble forming, though, a bulky, non-structured film (see the Experimental Section). The passivation effect of alumina was much less effective and the PL could only be preserved up to 20% of its maximum after 60 ALD cycles (Figure 4b). Since the porosity of the Si-NC assembly in the film was identical to that in the inverse opal, the open, well-ordered volume distribution in the inverse opal was critical for the efficient NCs passivation. It is worth noting that, without alumina passivation (0 cycles), the PL degradation in the non-structured film is lower than that measured in the bare Si-NC opal (Figure 4b). This suggests that the bulky character of the film provided some protection against quenching, although it simultaneously hindered posterior passivation.

Finally, two further aspects must be noted. First, alumina passivation of opal (b), i.e., without HF-etching of remnant silica, was clearly less effective than that measured in opal (d) (Figure 4b). This indicates that remnant silica, adjoining to the formed Si-NCs, hindered the access to their surface rather than native silica did. Second, aging was dramatic in non-passivated opals: PL emission strongly reduced its intensity (~20-fold) and blue-shifted (center at 570 nm) in opals (b,c) after 12 months. By contrast, aging was largely prevented by the presence of MgO in opal (a) or by deposited alumina in opal (d), so that PL barely changed within 18 months after fabrication.

In conclusion, we have prepared 3D-nanostructured ensemble of Si-NCs forming inverse opals by a straightforward magnesiothermic process. Si-NCs opals exhibited light emission, even observable with the naked eye, in a broadband ranging from 500 to 1050 nm. The photoluminescence, which strongly diminished under photoexcitation, could be preserved to a large extent by engineering the interface of the NCs (or their ensembles) with direct deposition of alumina, accurately controlled by ALD. The formation of abundant silicon suboxides was confirmed, probably contributing to the chemical passivation of Si-NCs surface. The high accessibility of the nanocrystals throughout the whole structure was a key factor for the efficient

PL stabilization. Si-NCs here prepared are self-supported and nanostructured in a single procedure, which is advantageous in terms of fabrication and incorporation in potential photonic or sensing devices.[25] Further, future investigation should explore light emission enhancement at the opal stop-band, profiting of the high refractive index contrast and tunability of such silicon/air photonic structures.[26]

Experimental Section

PS opals, made by 940 nm spheres (Duke Scientific) on silicon substrates, were infiltrated by SiO_2 chemical vapor deposition and PS calcination to obtain silica inverse opals[27] with (45 ± 5) nm thick walls (filling fraction of ~70% of the pore). Opal magnesiothermic reduction was carried out in a stainless steel reactor constituted by two chambers separated 10 cm, one having magnesium powder; the other one, the silica opals. The reactor was then sealed under Argon (4 N) atmosphere in a glove box and introduced into a muffle furnace, ramped to 700 °C in 1.5 h and then held at this temperature for 2 h. Opals were then immersed in a 1 M HCl aqueous solution for 6 h to remove the magnesia. HF etching during 5 min, followed by water/ethanol rinsing, removed the remnant SiO_2 to obtain a bare Si-NC inverse opals. Outside the starting PS opals (where no structure was present), the fabrication process led to formation of non-structured Si-NC thin films.

Alumina infiltration was performed with an ALD system (Savannah 100 & 200, Cambridge NanoTech Inc.). Reactants for alumina growth, i.e., trimethylaluminum (TMA) and water, were kept at room temperature. The sample, in the ALD vacuum chamber at 350 °C, was exposed to an initial TMA pulse followed by alternating TMA and water pulses (10 ms long each) in this order. Each TMA-water cycle was followed by a waiting time of 5 s, to ensure complete diffusion through the sample, and by chamber evacuation for 5 s. The rate of alumina growth was about 0.1 nm per cycle, as estimated by ellipsometry measurements.

Field emission SEM and EDX analysis were performed with a FEI Nova NANOSEM 230. HRTEM images were obtained with a JEOL 2011 microscope at 200 kV in samples previously thinned down to <200 nm by focused ion beam (FEI Quanta200 3D). Optical characterization was performed in a Fourier transform infrared spectrometer (IFS 66S Bruker) with an IR microscope attached. XPS spectra were recorded with a hemispherical electron spectrometer (SPECS Phoibos 150) using monochromatic Al Kα radiation (1486.74 eV). The photoelectron take-off angle was 90°. High resolution spectra were acquired with 10 eV pass energy providing an overall resolution of 0.40 eV.

PL was recorded by an Ocean 2000+ spectrometer under photoexcitation by a 488 nm Ar^+ laser beam focused to a spot of about 0.05 mm^2 (~2 W cm^{-2}). The external incidence angle of the beam was 40° (about 20°, internal) with respect to the normal of the sample in order to avoid the reflected laser light reaching the spectrometer. Scattered laser light was further blocked with an edge filter placed before the spectrometer. The time acquisition of the spectra was 2 ms, which is shorter than the response time of our system.

Acknowledgements

This work was partially supported by EU FP7 NoE Nanophotonics4Energy grant No. 248855; the Spanish MICINN CSD2007-0046 (Nanolight.es), CSD2008-00023 (FUNCOAT), CSD2009-00013 (Imagine), MAT2009-07841 (GLUSFA), TEC2008-06756-C03-02/TEC, CSIC PIF08-016 (Intramural Frontera), MAT2010-18432 and the Comunidad de Madrid S2009/MAT-1756 (PHAMA) projects. F. G. G. was supported by the JAE Postdoctoral Program from the CSIC. M. I. is a Ramón y Cajal researcher. We also thank A. Valera for SEM characterization at ICMM.

Received: May 13, 2011
Published online: September 8, 2011

[1] A. G. Cullis, L. T. Canham, P. D. J. Calcott, *J. Appl. Phys. Lett.* **1997**, *82*, 909.
[2] N. Daldosso, L. Pavesi, *Laser Photon. Rev.* **2009**, *3*, 508.
[3] R. J. Walters, R. V. A. van Loon, I. Brunets, J. Schmitz, A. Polman, *Nat. Mater.* **2010**, *9*, 21.
[4] D. Liang, J. E. Bowers, *Nat. Photon.* **2010**, *4*, 511.
[5] M. J. Sailor, E. C. Wu, *Adv. Funct. Mater.* **2009**, *19*, 3195.
[6] N. O'Farrell, A. Houlton, B. R. Horrocks, *Int. J. Nanomed.* **2006**, *1*, 451.
[7] S. Godefroo, M. Hayne, M. Jivanescu, A. Stesmans, M. Zacharias, O. I. Lebedev, G. van Tendeloo, V. V. Moshchalkov, *Nat. Nanotechnol.* **2008**, *3*, 174.
[8] W. D. A. M. de Boer, D. Timmerman, K. Dohnalova, I. N. Yassievich, H. Zhang, W. J. Buma, T. Gregorkiewicz, *Nat. Nanotechnol.* **2010**, *5*, 878.
[9] M. V. Wolkin, J. Jorne, P. Fauchet, G. Allan, C. Delerue, *Phys. Rev. Lett.* **1999**, *82*, 197.
[10] M. D. Mason, G. M. Credo, K. D. Weston, S. K. Buratto, *Phys. Rev. Lett.* **1998**, *80*, 5405.
[11] F. Cichos, J. Martin, C. von Borczyskowski, *Phys. Rev. B* **2004**, *70*, 115314.
[12] R. J. Rostron, Y. Chao, G. Roberts, B. R. Horrocks, *J. Phys. Condens. Matter.* **2009**, *21*, 235301.
[13] T. Tamura, S. Adachia, *J. Appl. Phys.* **2009**, *105*, 113518.
[14] J. Heitmann, F. Müller, M. Zacharias, U. Gösele, *Adv. Mater.* **2005**, *17*, 795.
[15] R. J. Walters, G. I. Bourianoff, H. A. Atwater, *Nat. Mater.* **2005**, *4*, 143.
[16] Z. Bao, M. R. Weatherspoon, S. Shian, Y. Cai, P. D. Graham, S. M. Allan, G. Ahmad, M. B. Dickerson, B. C. Church, Z. Kang, H. W. Abernathy III, C. J. Summers, M. Liu, K. H. Sandhage, *Nature* **2007**, *446*, 172.
[17] E. K. Richman, C. B. Kang, T. Brezesinski, S. H. Tolbert, *Nano Lett.* **2008**, *8*, 3075.
[18] M. Ibisate, D. Golmayo, C. López, *Adv. Mater.* **2009**, *21*, 2899.
[19] B. Hatton, L. Mischenko, S. Davis, K. H. Sandhage, J. Aizenber, *Proc. Nat. Acad. Sci. USA* **2010**, *107*, 10354.
[20] E. Sun, F.-H. Su, C.-H. Chen, M.-J. Chen, *Appl. Surf. Sci.* **2010**, *256*, 5021.
[21] Y. Cai, S. M. Allan, K. H. Sandhage, F. M. Zalar, *J. Am. Ceram. Soc.* **2005**, *88*, 2005.
[22] J. Valenta, A. Fucikova, F. Vácha, F. Adamec, J. Humpoícková, M. Hof, I. Pelant, K. Kusová, K. Dohnalová, J. Linnros, *Adv. Funct. Mater.* **2008**, *18*, 2666.
[23] G. Ledoux, O. Guillois, D. Porterat, C. Reynaud, F. Huisken, B. Kohn, V. Paillard, *Phys. Rev. B* **2000**, *62*, 15942.
[24] F. J. Himpsel, F. R. McFeely, A. Talev-Ibrahimi, J. A. Yarmoff, G. Hollinger, *Phys. Rev. B* **1988**, *38*, 6084.
[25] Y. Cohen, B. Hatton, H. Míguez, N. Coombs, S. Fournier-Bidoz, J. K. Grey, R. Beaulac, C. Reber, G. A. Ozin, *Adv. Mater.* **2003**, *15*, 572.
[26] A. Blanco, E. Chomski, S. Grabtchak, M. Ibisate, S. John, S. W. Leonard, C. Lopez, F. Meseguer, H. Miguez, J. P. Mondia, G. A. Ozin, O. Toader, H. M. van Driel, *Nature* **2000**, *405*, 437.
[27] A. Blanco, C. López, *Adv. Mater.* **2006**, *18*, 1593.